Advances in Science and Technology Research Journal

Advances in Science and Technology Research Journal, 18(8), 125–141
https://doi.org/10.12913/22998624/194145
ISSN 2299-8624, License CC-BY 4.0

Received: 2024.08.16
Accepted: 2024.10.04
Published: 2024.11.01

Free Vibration Analysis of Prestressed Timoshenko Beams Using the Modal Analysis Method

Sy Nam Nguyen[1], Xuan Cuong Nguyen[1*], Trung Hieu Nguyen[2]

[1] Hanoi University of Civil Engineering, Hanoi, Vietnam
[2] Viet Architecture Joint Stock Company, Hanoi, Vietnam
* Corresponding author's e-mail: cuongnx@huce.edu.vn

ABSTRACT

Natural frequency and mode shape are important features in the dynamic analysis of beam structures. They are used in the analysis, design, and verification of beam structures. In dynamic problems, these characteristics influence the dynamic response of the beam. This study presents the equations for the free vibration analysis of prestressed Timoshenko beams and derives the characteristic equations to determine the natural frequencies and general mode functions using the modal analysis method. For each different boundary condition of the beam, the corresponding characteristic equations and eigenforms are then obtained. Using numerical methods, the change in natural frequencies is investigated and compared with the natural frequencies of ordinary Timoshenko beams and Euler-Bernoulli beams. As the beams undergo pre-compression, the gap in natural frequencies between the prestressed Timoshenko beam and the unstressed beam widens with increasing prestress. The natural frequency of the pre-tensioned beam is higher than that of the beam without pre-tension. This difference is most noticeable at the first order of the frequency, where it is most significant, but it decreases quickly as the frequency order rises.

Keywords: natural frequency, mode shape, prestressed beam, Timoshenko beam, modal function.

INTRODUCTION

For a long time, Timoshenko (TM) beam theory has been widely used [1–5] for the static and dynamic analysis of elastic structures, such as beams, concrete bridges, railway bridges, and more. Unlike EulerBernoulli (EB) beam theory [6], which ignores shear deformation and rotational inertia, TM beam theory includes both factors. Therefore, it is not possible to establish an analytic relationship between shear force and moment in the TM beam. TM beams are also known as thick beam theory or second-order beam theory.

If the transverse bending vibration of the EB beam is described by a partial differential equation of deflection, then the vibrational equations of the TM beam are two partial differential equations corresponding to two unknowns that need to be determined: the transverse displacement and the rotation angle due to pure bending [7–9]. To analyze the natural frequencies and mode functions, the equations of free vibration are used (with the right-hand sides set to zeros). To analyze forced vibration, the right-hand side equations are often used. There are various methods for studying these problems, such as the Ritz method, finite element method (FEM) [10–12], finite difference method (FDM), and modal analysis method (MAM).

In the problems of structural verification and evaluation, the natural frequencies are characteristics that need to be determined. Studies have used piezoelectric accelerometers [13] and experimental investigations [14] to check the natural frequency and deflection of reinforced concrete beams when the reinforcement was corroded. The authors concluded that

changes in natural frequency could determine the extent of damage due to corrosion. The authors in [15–18] have shown that natural frequency and vibration patterns are inherent properties of beam structures. They are directly proportional to stiffness, inversely proportional to mass, and depend on boundary conditions. Any change in natural frequency indicates a change in structural properties, such as damage or enhancement. In [19], it was demonstrated that evaluating natural frequency is an easy and convenient method with valuable findings for assessing the overall structural condition.

Natural frequency and natural form are two characteristics of beams that are also used to analyze forced vibrations of beams using MAM [7–9, 20, 21]. Additionally, in dynamic problems, changes in frequencies can influence oscillation properties, potentially moving oscillations from the far-resonant region to the near-resonant region, or vice versa. Therefore, it is essential to define these characteristics. For ordinary beams, these characteristics have been studied quite extensively. However, for prestressed beams, which are reinforced by applying pre-tension or pre-compression forces to enhance load-bearing capacity, reduce bending, and decrease deflection, previous studies are less complete.

Prestressed EB beams have been the subject of many studies [22–33]. In [24], the impact of longitudinal force on the change in natural frequencies and mode shapes of prestressed EB beams was investigated using a beam model with two supports. In [25], it was shown that when a beam is pre-compressed, its frequency decreases, leading to a corresponding decrease in stiffness. This effect is referred to as "softening of beams due to pre-compression." Research in [26] used FEM combined with experiments to evaluate the effect of prestress on the natural frequencies of beams with free boundaries. In [27], the natural frequency and mode shapes of EB beams with cracks and prestressing were determined. Subsequently, reference [28] investigated the dynamic response of such beams under the action of a moving body. In [34], the authors demonstrated how to determine the natural frequency of simply supported prestressed concrete beams using STAAD.Pro, employing EB beam theory. The results were then compared with analytical solutions for unprestressed EB beams. They also showed that the frequency change increases as the order of oscillation increases.

In [35], the influence of the magnitude of the prestressing force on the natural frequency of beams (using EB beam theory) was investigated using mathematical tools. The study in [36] examined how prestress forces affect the modal characteristics of concrete beams. Research on prestressed TM beams is still limited. In [29], the authors used the reverberation-ray matrix approach to study the vibrations of prestressed Rayleigh-Timoshenko beams subjected to arbitrary forces. Reference [30] explored the free vibration of a PTM beam placed on a Winkler elastic foundation using FEM, but the natural frequencies were not determined in that study.

Prestressed TM beams, subjected to tension or compression, are very common in practice, especially in concrete structures. The traditional steel beam is heavier than the prestressed steel beam with the same dimensions and load capacity [37]. Furthermore, the span and load-carrying capacity of beams can be improved through prestressing. Therefore, prestressed structures have been applied not only to new constructions but also to existing ones, such as bridges, aircraft, and so on [38–40]. Therefore, it is necessary to consider changes in the natural frequency law due to prestressing factors. However, this issue has not yet been thoroughly studied because the complexity of the prestressed TM beam model makes it a challenging problem. In this study, the vibration equations for prestressed TM beams are examined using the MAM method, and the characteristic equations and general mode functions are obtained. By substituting the boundary conditions into the general form, this study also derives the formula for each beam corresponding to each boundary condition. The Newton-Raphson method can then be used to solve the nonlinear algebraic characteristic equations that determine the natural frequencies of the beams.

GENERAL EQUATIONS

Vibration equations of the prestressed Timoshenko beam

Considering the PTM beam model as shown in Figure 1. The geometric axis of the beam remains straight without deformation. Neglect torsional and axial vibrations. Beams only perform bending vibrations under the action of distributed force. Thus, transverse displacement, cross-sectional rotation, bending moment, and shear force are functions of the x-coordinate and t-time, they are denoted by $w(x,t),\varphi(x,t),M(x,t)$ and $Q(x,t)$ respectively.

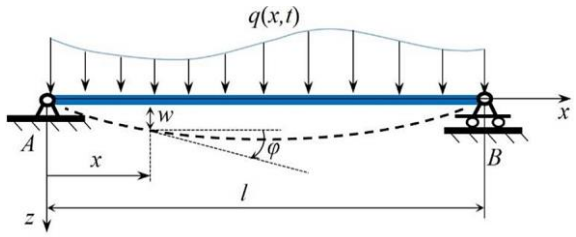

Figure 1. Beam subjected to distributed force

For the TM beam, the cross-section's rotation angle (φ) equals the total of the rotation angles brought on by the bending strain (ϕ) and the shear strain (γ). For EB beams, the angle component is zero due to ignoring the effect of shear strain.

$$\tan\varphi = \frac{\partial w}{\partial x} \approx \varphi = \phi + \gamma \tag{1}$$

The transverse vibration equations of the beam [7–9, 20, 21] have the form:

$$\rho A(x)\frac{\partial^2 w(x,t)}{\partial t^2} - \frac{\partial Q(x,t)}{\partial x} = q(x,t) \tag{2}$$

$$\rho I(x)\frac{\partial^2 \phi(x,t)}{\partial t^2} + \frac{\partial M(x,t)}{\partial x} - Q(x,t) = \tau(x,t) \tag{3}$$

where: $A(x)$ and $I(x)$ are the area and inertia moment of cross-sectional respectively, and ρ is the mass density.

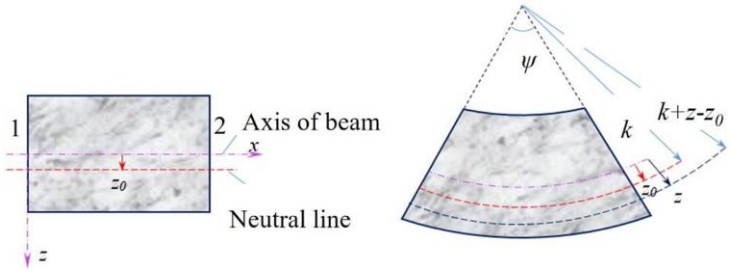

Figure 2. Normal strain of a beam segment

Considering a beam segment as shown in Fig. 2, the bending moment and shear force are determined by the formula [41]:

$$M = \int_A z\sigma_{xx}dA\,;\; Q = \kappa GA(x)\gamma = \kappa GA(x)\left(\frac{\partial w}{\partial x} - \phi\right) \tag{4}$$

where: G is the shear modulus and κ is the correction shear factor.

In the case of TM beams. The axial stress is determined by Hook's law in the form:

$$\sigma_{xx} = E\varepsilon_{xx}(x,z,t);\ \varepsilon_{xx}(x,z,t) = -z\frac{\partial\phi}{\partial x} \tag{5}$$

where: E is Young's modulus, ε_{xx} is the normal strain of the beam due to bending displacement.

Substituting expressions (4) and (5) into Equations 2 and 3 we get:

$$\rho A\frac{\partial^2 w(x,t)}{\partial t^2} - \kappa GA\left(\frac{\partial^2 w(x,t)}{\partial^2 x} - \frac{\partial\phi(x,t)}{\partial x}\right) = q(x,t) \tag{6}$$

$$\rho I\frac{\partial^2\phi(x,t)}{\partial t^2} = \kappa GA\left(\frac{\partial w(x,t)}{\partial x} - \phi\right) + EI\frac{\partial^2\phi(x,t)}{\partial x^2} \tag{7}$$

Thus, we obtain two partial differential equations of ordinary Timoshenko beams with two unknowns $w(x, t)$ and $\phi(x, t)$. In the case of PTM beams, the normal strain $\varepsilon_{xx}(x, z, t)$ in the x-direction:

$$\varepsilon_{xx}(x,z,t) = \varepsilon_0(x) + \varepsilon^*_{xx}(x,z,t) \tag{8}$$

where $\varepsilon_0(x)$ is the initial normal strain caused by prestressing. Considering the position of the cross-section with x-coordinates, the proportional long strain is:

$$\varepsilon_0(x,z,0) = \varepsilon_0(x) \tag{9}$$

here $\varepsilon^*_{xx}(x,z,t)$ is the normal strain added when the beam is deformed. These strains are linear in the elastic domain, and the initial strain from prestressing and the strain from bending together make up the total normal strain.

Substituting Equation 5 into Equation 8, ignoring the higher-order infinity, we have:

$$\varepsilon_{xx}(x, z,t) = \varepsilon_0(x) - z\frac{\partial\phi}{\partial x} \tag{10}$$

Substituting Equation 10 into Equation 4 we get:

$$M = E\varepsilon_0\int_A zdA - E\frac{\partial\phi}{\partial x}\int_A z^2 dA \tag{11}$$

The following equations are used to calculate the z_C - coordinate (center of the dx-element) and the inertia moment of inertia of the cross-section:

$$Az_C = \int_A zdA\ ;\ I(x) = \int_A z^2 dA \tag{12}$$

If the beam is not deformed, $z_C = 0$, and if it is deformed, $z_C = w$.
Substituting Equation 12 into Equation 11, we get:

$$M(x,t) = EA(x)\varepsilon_0 w - EI(x)\frac{\partial\phi}{\partial x} \tag{13}$$

Assume that the neutral axis and the axis of symmetry are the same, and by substituting Equation 4 and Equation 13 into Equation 2 and Equation 3, the cross-section of the beam is constant, and the beam is homogeneous, then A, I, and ε_0 are constants.

The motion equations have the form:

$$\rho A\frac{\partial^2 w(x,t)}{\partial t^2} - \kappa GA\left(\frac{\partial^2 w}{\partial x^2} - \frac{\partial\phi}{\partial x}\right) = q(x,t) \tag{14}$$

$$\rho I(x)\frac{\partial^2\phi(x,t)}{\partial t^2} - EI\frac{\partial^2\phi}{\partial x^2} - \kappa GA\left(\frac{\partial w}{\partial x} - \phi\right) + \varepsilon_0 EA\frac{\partial w}{\partial x} = 0 \tag{15}$$

Eigenvalues and mode functions

Free vibration equations of the PTM beam have the form:

$$\rho A\frac{\partial^2 w(x,t)}{\partial t^2}-\kappa GA\left(\frac{\partial^2 w}{\partial x^2}-\frac{\partial \phi}{\partial x}\right)=0 \tag{16}$$

$$\rho I(x)\frac{\partial^2 \phi(x,t)}{\partial t^2}-EI\frac{\partial^2 \phi}{\partial x^2}-\kappa GA\left(\frac{\partial w}{\partial x}-\phi\right)+\varepsilon_0 EA\frac{\partial w}{\partial x}=0 \tag{17}$$

For normal TM beams, their solutions have the variable dissociation [7, 8], according to the expression:

$$w(x,t)=W(x).T(t) \tag{18}$$

$$\phi(x,t)=\Phi(x).T(t) \tag{19}$$

For PTM beams, we use a lemma to prove the ability to dissociate solutions. Taking the derivative of Equation 17 concerning the variable *x*, and then substituting it into Equation 16, we get:

$$\rho I\frac{\partial^3 \phi(x,t)}{\partial x\partial t^2}+\varepsilon_0 EA\frac{\partial w^2(x,t)}{\partial x^2}-EI\frac{\partial \phi^3(x,t)}{\partial x^3}-\rho A\frac{\partial^2 w(x,t)}{\partial t^2}=0 \tag{20}$$

From Equation 16, we can also derive:

$$\frac{\partial \phi}{\partial x}=\frac{\partial^2 w}{\partial x^2}-\frac{\rho A}{\kappa GA}\frac{\partial^2 w(x,t)}{\partial t^2} \tag{21}$$

From Equation 21, we can calculate the derivatives:

$$\frac{\partial^3 \phi}{\partial x^3}=\frac{\partial^4 w}{\partial x^4}-\frac{\rho A}{\kappa GA}\frac{\partial^4 w(x,t)}{\partial x^2\partial t^2};\ \frac{\partial^3 \phi}{\partial x\partial t^2}=\frac{\partial^4 w}{\partial x^2\partial t^2}-\frac{\rho A}{\kappa GA}\frac{\partial^4 w(x,t)}{\partial t^4} \tag{22}$$

Substituting Equation 22 into Equation 20 we have:

$$\begin{aligned}&\rho I\left(\frac{\partial^4 w}{\partial x^2\partial t^2}-\frac{\rho A}{\kappa GA}\frac{\partial^4 w(x,t)}{\partial t^4}\right)+\varepsilon_0 EA\frac{\partial^2 w(x,t)}{\partial x^2}\\&-EI\left(\frac{\partial^4 w}{\partial x^4}-\frac{\rho A}{\kappa GA}\frac{\partial^4 w(x,t)}{\partial x^2\partial t^2}\right)-\rho A\frac{\partial^2 w(x,t)}{\partial t^2}=0\end{aligned} \tag{23}$$

Simplifying we get a partial derivative of the fourth order of $w(x,t)$:

$$\begin{aligned}&-EI\frac{\partial^4 w}{\partial x^4}+\rho I\left(1+\frac{E}{\kappa G}\right)\frac{\partial^4 w(x,t)}{\partial x^2\partial t^2}-\frac{\rho^2 I}{\kappa G}\frac{\partial^4 w(x,t)}{\partial t^4}+\varepsilon_0 EA\frac{\partial w^2(x,t)}{\partial x^2}\\&-\rho A\frac{\partial^2 w(x,t)}{\partial t^2}=0\end{aligned} \tag{24}$$

Continuing the first-order derivative of Eq. (17) for the *x*-variable, we get:

$$\rho A\frac{\partial^3 w}{\partial x\partial t^2}-\kappa GA\left(\frac{\partial^3 w}{\partial x^3}-\frac{\partial^2 \phi}{\partial x^2}\right)=0 \tag{25}$$

From Equation 15, we derive the components and their derivatives. After that by substituting into Equation 25, the same transformation, we have:

$$-EI\frac{\partial^4 \phi}{\partial x^4}+\rho I\left(\frac{E}{\kappa G}+1\right)\frac{\partial^4 \phi}{\partial t^2\partial x^2}-\frac{\rho^2 I}{\kappa G}\frac{\partial^4 \phi}{\partial t^4}+\varepsilon_0 EA\frac{\partial^2 \phi}{\partial x^2}-\rho A\frac{\partial^2 \phi}{\partial t^2}=0 \tag{26}$$

Thus, Equation 24 and 26 are dissociation equations written for each variable. Moreover, these equations have the same form. Therefore, the solutions Equation 18 and 19 are still valid for RTM beams. Derivative from Equation 18 and 19 and substituting into the Equation 16 and 17, we get:

$$\frac{\kappa G}{\rho}\frac{W''(x)}{W(x)}-\frac{\kappa G}{\rho}\frac{\Phi'(x)}{W(x)}=\frac{\ddot{T}(t)}{T(t)} \tag{27}$$

$$-\frac{\varepsilon_0 EAW'(x)}{\rho I\Phi(x)}+\frac{EI\Phi''(x)}{\rho I\Phi(x)}+\frac{\kappa GAW'(x)}{\rho I\Phi(x)}-\frac{\kappa GA}{\rho I}=\frac{\ddot{T}(t)}{T(t)} \tag{28}$$

Since the right sides of Equation 27 and 28 depend on t and their left sides depend on x, both sides must be constants. Hence, we put:

$$\frac{\ddot{T}(t)}{T(t)} = -\omega^2 \tag{29}$$

Substituting Equation 28 into Equation 26 and 27, we get:

$$\kappa G W''(x) - \kappa G \Phi'(x) + \omega^2 \rho W(x) = 0 \tag{30}$$

$$EI\Phi''(x) + (\kappa GA - \varepsilon_0 EA) W'(x) + \left(\omega^2 \rho I - \kappa GA\right)\Phi(x) = 0 \tag{31}$$

From Equation 30, we have:

$$\Phi'(x) = W''(x) + \frac{\omega^2 \rho}{\kappa G} W(x) \tag{32}$$

Deriving Equation 31 concerning x and then substituting 31 into that result, we get the Equation:

$$W^{(4)} + \left(\left(\frac{1}{\kappa G} + \frac{1}{E}\right)\rho\omega^2 - \frac{\varepsilon_0 A}{I}\right) W'' + \omega^2 \rho \left(\frac{\omega^2 \rho}{E\kappa G} - \frac{A}{EI}\right) W = 0 \tag{33}$$

The characteristics of Equation 33 are:

$$\lambda^4 + b\lambda^2 + c = 0 \tag{34}$$

with
$$b = \left(\frac{1}{\kappa G} + \frac{1}{E}\right)\rho\omega^2 - \frac{\varepsilon_0 A}{I};\ c = \rho\omega^2 \left(\frac{\omega^2 \rho}{E\kappa G} - \frac{A}{EI}\right) \tag{35}$$

Replacing $k = \lambda^2$, we have the Equation:

$$k^2 + bk + c = 0 \tag{36}$$

If $c = 0$ then:

$$\frac{\omega^2 \rho}{E\kappa G} - \frac{A}{EI} = 0 \Rightarrow \omega = \sqrt{\frac{\kappa GA}{\rho I}} = \omega_c \tag{37}$$

The symbol ω_c is called *cut-off* frequency. This is a mathematical value; practically, no natural frequency of a beam will be equal to this value.

If $c \neq 0$ then the delta determinant of Equation 36 is positive definite:

$$\begin{aligned} \Delta &= \left(\left(\frac{1}{\kappa G} + \frac{1}{E}\right)\rho\omega^2 - \frac{\varepsilon_0 A}{I}\right)^2 - 4\omega^2 \rho \left(\frac{\omega^2 \rho}{E\kappa G} - \frac{A}{EI}\right) \\ \Leftrightarrow \Delta &= \left(\frac{\varepsilon_0 A}{I} - \left(\frac{1}{\kappa G} - \frac{1}{E}\right)\rho\omega^2\right)^2 + \frac{4A}{EI}(1 - \varepsilon_0)\rho\omega^2 \end{aligned} \tag{38}$$

Due to $|\varepsilon_0| \ll 1$, then $\Delta > 0$. The solutions of Eq. (35) are:

$$k_1 = \frac{-b + \sqrt{\Delta}}{2};\ k_2 = \frac{-b - \sqrt{\Delta}}{2} \tag{39}$$

We consider two frequency regions:

In frequency region $\omega < \omega_c$: From Equation 35 and Equation 37, deducing $c < 0$. Since $k = \lambda^2$, we have:

$$k_1 = \frac{-b + \sqrt{\Delta}}{2} > 0 \Rightarrow \lambda_1 = \beta,\ \lambda_2 = -\beta (\beta > 0) \tag{40}$$

and
$$k_2 = \frac{-b - \sqrt{\Delta}}{2} < 0 \Rightarrow \lambda_1 = i\xi,\ \lambda_2 = -i\xi \tag{41}$$

In frequency region $\omega > \omega_c$: From Equation 35 and Equation 37, deducing $c < 0$. We have:

$$\begin{aligned} k_1 &= \frac{-b + \sqrt{\Delta}}{2} < 0 \Rightarrow \lambda_1 = i\eta,\ \lambda_2 = -i\eta \\ k_2 &= \frac{-b - \sqrt{\Delta}}{2} < 0 \Rightarrow \lambda_3 = i\xi,\ \lambda_4 = -i\xi \end{aligned} \tag{42}$$

$$\beta=\frac{\sqrt{-b+\sqrt{\Delta}}}{\sqrt{2}};\ \xi=\frac{\sqrt{b+\sqrt{\Delta}}}{\sqrt{2}};\ \eta=\frac{\sqrt{b-\sqrt{\Delta}}}{\sqrt{2}}$$

The solutions of Equation 30 and 31 are determined according to the four eigenvalues: $\lambda_1, \lambda_2, \lambda_3, \lambda_4$, as follows:

In frequency region $\omega < \omega_c$: The form of the solutions:

$$W(x) = C_1e^{\lambda_1 x}+C_2e^{\lambda_2 x}+C_3e^{\lambda_3 x}+C_4e^{\lambda_4 x}=C_1e^{\beta x}+C_2e^{-\beta x}+C_3e^{i\xi x}+C_4e^{-i\xi x} \quad (43)$$

$$W(x) = C_1e^{\lambda_1 x}+C_2e^{\lambda_2 x}+C_3e^{\lambda_3 x}+C_4e^{\lambda_4 x}=C_1e^{\beta x}+C_2e^{-\beta x}+C_3e^{i\xi x}+C_4e^{-i\xi x} \quad (44)$$

Using Euler's formulas, we get the trigonometric form:

$$W(x) = a_1\sinh\beta x+a_2\cosh\beta x+a_3\sin\xi x+a_4\cos\xi x \quad (45)$$

$$\Phi(x)= d_1\sinh\beta x+d_2\cosh\beta x+d_3\sin\xi x+d_4\cos\xi x \quad (46)$$

where: the constants a_i and d_i (i = 1, 2, 3, 4) are determined by the boundary conditions. The constants a_i and d_i are also not independent since the functions $W(x)$and $\Phi(x)$ are not independent.

Substituting Equation 45 and 46 into Equation 30, identifying the trigonometric functions on both sides, we get:

$$\left(\kappa G a_1\beta^2-\kappa G d_2\beta+\omega^2\rho\, a_1\right)=0 \Rightarrow d_2=a_1\left(\beta+\frac{\omega^2\rho}{\kappa G\beta}\right)=a_1h_\beta \quad (47)$$

$$\left(\kappa G a_2\beta^2-\kappa G d_1\beta+\omega^2\rho\, a_2\right)=0 \Rightarrow d_1=a_2\left(\beta+\frac{\omega^2\rho}{\kappa G\beta}\right)=a_2h_\beta \quad (48)$$

$$\left(-a_3\xi^2\kappa G+\kappa G d_4\xi+\omega^2\rho\, a_3\right)=0 \Rightarrow d_4=a_3\left(\xi-\frac{\omega^2\rho}{\kappa G\xi}\right)=a_3f_\xi \quad (49)$$

$$\left(-\kappa G a_4\xi^2-\kappa G d_3\xi+\omega^2\rho\, a_4\right)=0 \Rightarrow d_3=-a_4\left(\xi-\frac{\omega^2\rho}{\kappa G\xi}\right)=-a_4f_\xi \quad (50)$$

where $$h_\beta=\left(\beta+\omega^2\rho/(\kappa G\beta)\right);\ f_\xi=\left(\xi-\omega^2\rho/(\kappa G\xi)\right) \quad (51)$$

Substituting equations from Equation 47 to Equation 50 into Equation 46, we get the mode functions:

$$W(x) = a_1\sinh\beta x+a_2\cosh\beta x+a_3\sin\xi x+a_4\cos\xi x \quad (52)$$

$$\Phi(x) = a_2h_\beta\sinh\beta x+a_1h_\beta\cosh\beta x-a_4f_\xi\sin\xi x+a_3f_\xi\cos\xi x \quad (53)$$

In frequency region $\omega > \omega_c$: The form of the solutions:

$$W(x) = C_1e^{i\eta x}+C_2e^{-i\eta x}+C_3e^{i\xi x}+C_4e^{-i\xi x} \quad (54)$$

$$\Phi(x)=C_1'e^{i\eta x}+C_2'e^{-i\eta x}+C_3'e^{i\xi x}+C_4'e^{-i\xi x} \quad (55)$$

Using Euler's formulas to trigonometric form and similar transformations, we get mode functions:

$$W(x) = b_1\sin\eta x+b_2\cos\eta x+b_3\sin\xi x+b_4\cos\xi x \quad (56)$$

$$\Phi(x) = -b_2f_\eta\sin\eta x+b_1f_\eta\cos\eta x-b_4f_\xi\sin\xi x+b_3f_\xi\cos\xi x \quad (57)$$

where $$f_\eta=\left(\eta-\omega^2\rho/(\kappa G\eta)\right) \quad (58)$$

Thus, the mode functions of the PTM beam are determined by Equation 52 and Equation 53 in case $\omega < \omega_c$, and by Equation 56 and Equation 57 in case of $\omega > \omega_c$.

CALCULATION OF NATURAL FREQUENCIES AND MODE SHAPES

Simply supported PTM beam

Based on the boundary conditions of each type of beam, the characteristic equation and particular mode functions can be derived from the general mode functions, as shown in the system of equations from Equation 52 to Equation 57. As illustrated in Figure 1, The simply supported (SS) PTM beam has both transverse displacement and bending moment equal zeros at $x = 0$ and $x = l$:

$$w(0,t)= 0;\ M(0,t)=EA\varepsilon_0w(0)-EI\frac{\partial\phi(0)}{\partial x}=0 \quad (59)$$

$$w(l,t)= 0;\ M(l,t)=EA\varepsilon_0 w(l)-EI\frac{\partial\phi(l)}{\partial x}=0 \quad (60)$$

Substituting Equation 18 and Equation 19 into Equation 59 and Equation 60, we obtain:

$$W(0)=0;\ \Phi'(0)=0;\ W(l)=0;\ \Phi'(l)=0 \quad (61)$$

In frequency region $\omega < \omega_c$:

The natural frequencies: Substituting Equation 52 and 53 into Equation 61, we get:

$$W(0) = a_2+a_4=0 \quad (62)$$

$$\Phi'(0) = \beta a_2 h_\beta-\xi a_4 f_\xi=0 \quad (63)$$

$$W(l) = a_1 \sinh\beta l+a_2 \cosh\beta l+a_3 \sin\xi l+a_4 \cos\xi l=0 \quad (64)$$

$$\Phi'(l) = \beta a_2 h_\beta \cosh\beta l+\beta a_1 h_\beta \sinh\beta l-\xi a_4 f_\xi \cos\xi l-\xi a_3 f_\xi \sin\xi l=0 \quad (65)$$

From Equation 62 and Equation 63, we have:

$$a_2=a_4=0 \quad (66)$$

Substituting Equation 66 into Equation 64 and Equation 65, we get:

$$a_1 \sinh\beta l+a_3 \sin\xi l=0 \quad (67)$$

$$\beta a_1 h_\beta \sinh\beta l-\xi a_3 f_\xi \sin\xi l=0 \quad (68)$$

Since the solutions a_1 and a_3 are non-zero, then there must be:

$$\begin{vmatrix} \sinh\beta l & \sin\xi l \\ \beta h_\beta \sinh\beta l & -\xi f_\xi \sin\xi l \end{vmatrix}=0 \Leftrightarrow \left(\xi f_\xi+\beta h_\beta\right)\sin\xi l \sinh\beta l=0 \quad (69)$$

Equation 69 is the characteristic equation, solving this equation, we obtain the natural frequencies $\omega_j < \omega_c$, ($j=1, 2,\ldots$). Mode shapes – multiplying both sides of the Equation 67 by ξf_ξ and then adding to Equation 68, we get:

$$a_1\left(\xi f_\xi+\beta h_\beta\right)\sinh\beta l=0 \quad (70)$$

From Equation 43 and Equation 51, we have $\xi f_\xi+\beta h_\beta=2\sqrt{\Delta}>0$ and $\sinh\beta l>0$

We infer that $a_1=0$. Therefore, to have a solution where $a_i \neq 0$ then $a_3 \neq 0$. Substituting $a_1=a_2=a_4=0$; $a_3 \neq 0$ into Equation 52 and Equation 53, we get the mode shapes:

$$W(x) = a_3 \sin(j\pi x/l);\ \Phi(x) = a_3 f_\xi \cos(j\pi x/l) \quad (71)$$

In frequency region $\omega > \omega_c$:

Natural frequency: Substituting Equation 56 and Equation 57 into Equation 61, using the same method as proved above, we get:

$$\left(\xi f_\xi-\eta f_\eta\right)\sin\eta l \sin\xi l=0 \quad (72)$$

Substituting Equation 42 into Equation 72 and solving it, we get the natural frequencies: $\omega_k > \omega_c$, ($k=1, 2,\ldots$). Mode shapes – from Equation 56 and Equation 57, using a similar method, we have:

$$W(x) = b_1 \sin(n\pi x/l);\ \Phi(x) = b_1 f_\eta \cos(n\pi x/l) \quad (73)$$

Numerical results

In [7], the characteristics of un-prestressed TM beams were investigated using a numerical-analytic method, and in [31], these characteristics of the EB beam were determined in analytical forms. Consequently, in this study, the results from references [7] and [31] are selected for comparison. Numerical calculations are performed with the set of parameters as shown in reference [7]: l = 1 m, $A = b \times h$ = 0.02 × 0.08 m^2, E = 2.1 × 10^{11} N/m^2, G = 8.1 × 1010 N/m^2, ρ = 7860 kg/m^3, κ = 0.5. According to Equation 37, we can determine the cut-off frequency, ω_c=98291.71 rad/s (15643.62 Hz), and the

number of natural frequencies, N_B less than the cut-off frequency, N_B = 73. To compare the numerical results with EB beam, we use the formula to determine the natural frequencies of EB beams [31]:

$$\omega_k = \left(\frac{k\pi}{l}\right)^2 \sqrt{\frac{EI}{\rho A}}, \text{ with } k = 1, 2, 3... \tag{74}$$

The mode shapes of transverse displacement and cross-sectional rotation of the SS PTM beam are depicted in Figures 3 and 4, respectively. Calculation results are indicated in Table 1.

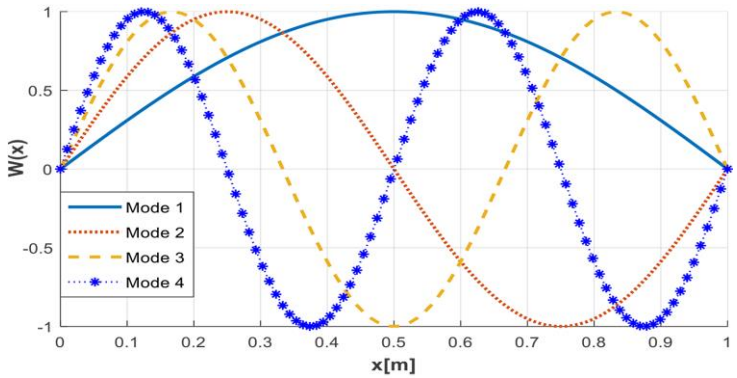

Figure 3. Mode shapes of the transverse displacement of the SS PTM beam

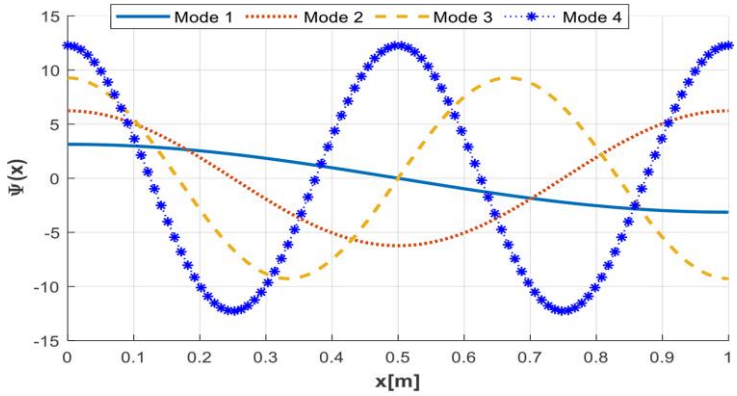

Figure 4. Mode shapes of the cross-sectional rotation of the SS PTM beam

As shown in Table 1, in the case without prestressing, the results for the TB beam show good agreement with those in reference [7]. It can be seen from Table 1 that, as the beam is subjected to pre-compression ($\varepsilon_0<0$), the natural frequencies of the PTM beams are reduced compared to those of the normal TM beams. The more compressed the beam, the lower the frequencies. This is called "softening"

Table 1. Natural frequencies of SS PTM beam

No.	EB [31] (rad/s)	TM (rad/s)		PTM (rad/s)			(b-a)/a (%)
		ε_0 = 0 (a)	[7]	$\varepsilon_0 = -10^{-4}$	$\varepsilon_0 = -5.10^{-4}$ (b)	$\varepsilon_0 = 10^{-4}$	
1	1178.141	1159.497	1159.4	1148.428	1103.046	1170.460	4.87
2	4712.566	4436.759	4436.8	4426.191	4383.668	4447.301	1.20
3	10603.274	9357.616	9357.6	9347.665	9307.755	9367.558	0.53
4	18850.265	15409.984	15410.0	15400.680	15363.412	15419.283	0.30
5	29453.539	22182.504	22183.0	22173.824	22139.071	22191.182	0.20
6	42413.096	29389.344	-	29381.241	29348.809	29397.446	0.14
7	57728.937	36845.603	-	36838.026	36807.706	36853.178	0.10
8	75401.061	44435.880	-	44428.781	44400.375	44442.979	0.08
9	95429.468	52089.639	-	52082.972	52056.300	52096.305	0.06
10	117814.15	59764.516	-	59758.242	59733.142	59770.789	0.05

in prestressed beams. When the beam is pre-tensioned ($\varepsilon_0>0$), its natural frequency increases compared to the normal beam. The natural frequencies of PTM beams and TM beams show the greatest difference at the first frequency (about 4.9% for $\varepsilon_0 = -5 \times 10^{-4}$). This discrepancy decreases rapidly as the frequency order increases. Under pre-compression ($\varepsilon_0 < 0$), the PTM beams deviate more from EB beams compared to when they are subjected to pre-tension ($\varepsilon_0 > 0$). For the same TM beam, the natural frequency under pre-compression is greater than that under pre-tension

Figures 3 and 4 illustrate four mode shapes of the natural frequency of the simply supported PTM beam under pre-compression ($\varepsilon_0 = -0.001$). These mode shapes are appropriate for this type of boundary condition.

Clamped–free PTM beam

Boundary conditions of the clamped–free (CF) PTM beam are displayed in Figure 5. At $x = 0$, the displacement and rotation are both zero:

$$w(0,t)=0 \Rightarrow W(0)=0;\ \phi(0,t)=0 \Rightarrow \Phi(0)=0 \tag{75}$$

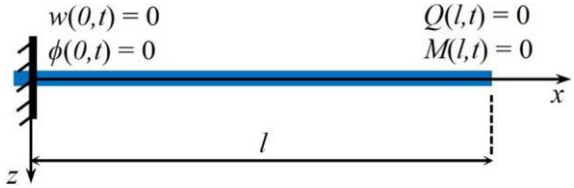

Figure 5. Clamped-free (CF) beam

At $x = l$, the torque and shear force are equal to zero, using the same method as indicated in the simply supported PTM beam, we have:

$$\begin{aligned} EA\varepsilon_0 w\text{-}EI\phi' &=0 \Rightarrow \frac{\varepsilon_0 A}{I} W(l)\text{-}\Phi'(l)=0 \\ \kappa GA[w'(l,t)\text{-}\phi(l,t)] &=0 \Rightarrow W'(l)\text{-}\Phi(l)=0 \end{aligned} \tag{76}$$

In frequency region $\omega < \omega_c$:

Natural frequency: Substituting the Equations 52 and 53 into Equations 75 and 76, we get:

$$a_2+a_4=0 \tag{77}$$

$$a_1 h_\beta+a_3 f_\xi=0 \tag{78}$$

$$\begin{aligned} &\left(\varepsilon_0 A/I\text{-}\beta h_\beta\right) a_1 \sinh\beta l+\left(\varepsilon_0 A/I\text{-}\beta h_\beta\right) a_2 \cosh\beta l+\left(\varepsilon_0 A/I+\xi f_\xi\right) a_3 \sin\xi l \\ &+\left(\varepsilon_0 A/I+\xi f_\xi\right) a_4 \cos\xi l=0 \end{aligned} \tag{79}$$

$$a_1(\beta\text{-}h_\beta)\cosh\beta l+a_2(\beta\text{-}h_\beta)\sinh\beta l+a_3\left(\xi\text{-}f_\xi\right)\cos\xi l\text{-}a_4\left(\xi\text{-}f_\xi\right)\sin\xi l=0 \tag{80}$$

From Equation 77 and Equation 78, we get:

$$a_4=\text{-}a_2,\ a_3=\text{-}a_1 h_\beta/f_\xi \tag{81}$$

Substituting Equation 81 into Equation 79 and Equation 80, we get:

$$\begin{aligned} &\left(\varepsilon_0 A/I\text{-}\beta h_\beta\right) a_1 \sinh\beta l+\left(\varepsilon_0 A/I\text{-}\beta h_\beta\right) a_2 \cosh\beta l\text{-} \\ &\left(\varepsilon_0 A/I+\xi f_\xi\right)\left(h_\beta/f_\xi\right) a_1 \sin\xi l\text{-}\left(\varepsilon_0 A/I+\xi f_\xi\right) a_2 \cos\xi l=0 \end{aligned} \tag{82}$$

$$\begin{aligned} &a_1(\beta\text{-}h_\beta)\cosh\beta l+a_2(\beta\text{-}h_\beta)\sinh\beta l\text{-}a_1\left(h_\beta/f_\xi\right)\left(\xi\text{-}f_\xi\right)\cos\xi l \\ &+a_2\left(\xi\text{-}f_\xi\right)\sin\xi l=0 \end{aligned} \tag{83}$$

For the solutions a_1 and a_2 to be non-zero, the following condition must hold:

$$\begin{vmatrix} \left(\varepsilon_0 A/I\text{-}\beta h_\beta\right)\sinh\beta l\text{-}\left(\varepsilon_0 A/I+\xi f_\xi\right)\left(h_\beta/f_\xi\right)\sin\xi l & \left(\varepsilon_0 A/I\text{-}\beta h_\beta\right)\cosh\beta l\text{-}\left(\varepsilon_0 A/I+\xi f_\xi\right)\cos\xi l \\ (\beta\text{-}h_\beta)\cosh\beta l\text{-}\left(h_\beta/f_\xi\right)\left(\xi\text{-}f_\xi\right)\cos\xi l & (\beta\text{-}h_\beta)\sinh\beta l+\left(\xi\text{-}f_\xi\right)\sin\xi l \end{vmatrix}=0$$

$$\Leftrightarrow \left[\left(\varepsilon_0 A/I-\beta h_\beta\right)\sinh\beta l-\left(\varepsilon_0 A/I+\xi f_\xi\right)\left(h_\beta/f_\xi\right)\sin\xi l\right]\left[\left(\beta-h_\beta\right)\sinh\beta l+\left(\xi-f_\xi\right)\sin\xi l\right]$$
$$-\left[\left(\varepsilon_0 A/I-\beta h_\beta\right)\cosh\beta l-\left(\varepsilon_0 A/I+\xi f_\xi\right)\cos\xi l\right]\left(\left(\beta-h_\beta\right)\cosh\beta l-\frac{h_\beta}{f_\xi}\left(\xi-f_\xi\right)\cos\xi l\right)=0 \quad (84)$$

Equation 84 is the characteristic equation that determines the natural frequency, which is a nonlinear algebraic equation. We determine the frequencies by solving Equation 84 using the Newton-Raphson method, where ω_j are the values to be determined: ω_j with $j=1, 2, \ldots$ such that $\omega_j<\omega_c$.

Mode shapes – from the Equation 82 and Equation 83, we deduce the coefficients corresponding to ω_j:

$$a_2^{(j)}=-a_1^{(j)}\frac{\left(\beta_j-h_\beta^{(j)}\right)\cosh\beta_j l-\frac{h_\beta^{(j)}}{f_\xi^{(j)}}\left(\xi_j-f_\xi^{(j)}\right)\cos\xi_j l}{\left(\beta_j-h_\beta^{(j)}\right)\sinh\beta_j l+\left(\xi_j-f_\xi^{(j)}\right)\sin\xi_j l}=-a_1^{(j)}g_j; \quad (85)$$

$$a_3^{(j)}=-a_1^{(j)}\frac{h_\beta^{(j)}}{f_\xi^{(j)}};\ a_4^{(j)}=-a_2^{(j)}=a_1^{(j)}g_j \quad (86)$$

in which

$$h_\beta^{(j)}=h_\beta(\omega_j);\ f_\xi^{(j)}=f_\xi(\omega_j);\ \xi_j=\xi(\omega_j);\ \beta_j=\beta(\omega_j); \quad (87)$$

$$g_j=\frac{\left(\beta_j-h_\beta^{(j)}\right)\cosh\beta_j l-\frac{h_\beta^{(j)}}{f_\xi^{(j)}}\left(\xi_j-f_\xi^{(j)}\right)\cos\xi_j l}{\left(\beta_j-h_\beta^{(j)}\right)\sinh\beta_j l+\left(\xi_j-f_\xi^{(j)}\right)\sin\xi_j l} \quad (88)$$

Substitute the coefficients in Eq. (52) and Eq. (53), we get mode shapes:

$$W_j(x)=a_1^{(j)}\left(\sinh\beta_j x+g_j\cosh\beta_j x-\left(h_\beta^{(j)}/f_\xi^{(j)}\right)\sin\xi_j x-g_j\cos\xi_j x\right) \quad (89)$$

$$\Phi_j(x)=a_1^{(j)}\left(h_\beta^{(j)}g_j\sinh\beta_j x+h_\beta^{(j)}\cosh\beta_j x+f_\xi g_j\sin\xi_j x-h_\beta^{(j)}\cos\xi_j x\right) \quad (90)$$

In frequency region $\omega > \omega_c$:

Natural frequency – substituting Equation 56 and Equation 57 into the boundary conditions Equation 75 and Equation 76, using the same method, we get:

The characteristic equation to determine the natural frequencies is:

$$\left[\left(\varepsilon_0 A/I+\eta f_\eta\right)\sin\eta l-\left(\varepsilon_0 A/I+\xi f_\eta\right)\left(f_\eta/f_\xi\right)\sin\xi l\right]\left[\left(\eta-f_\eta\right)\sin\eta l-\left(\xi-f_\xi\right)\sin\xi l\right]$$
$$+\left[\left(\varepsilon_0 A/I+\eta f_\eta\right)\cos\eta l-\left(\varepsilon_0 A/I+\xi f_\xi\right)\cos\xi l\right]\left(\left(\eta-f_\eta\right)\cos\eta l-\frac{f_\eta}{f_\xi}\left(\xi-f_\xi\right)\cos\xi l\right)=0 \quad (91)$$

Using the numerical method to solve the Equation 91, we will find the frequencies ω_k with $k = 1, 2,\ldots$ such that $\omega_k > \omega_c$.

Mode shapes – the mode shapes can be determined from the following equations:

$$W_k(x)=b_1^{(k)}\left(\sin\eta_k x+z_k\cos\eta_k x-\left(f_\eta^{(k)}/f_\xi^{(k)}\right)\sin\xi_k x-z_k\cos\xi x\right) \quad (92)$$

$$\Phi_k(x)=b_1^{(k)}\left(-z_k f_\eta^{(k)}\sin\eta_k x+f_\eta^{(k)}\cos\eta_k x+z_k f_\xi\sin\xi_k x-f_\eta^{(k)}\cos\xi x\right) \quad (93)$$

where

$$f_\eta^{(k)}=f_\eta(\omega_k);\ f_\xi^{(k)}=f_\xi(\omega_k);\ \xi_k=\xi(\omega_k);\ \beta_k=\beta(\omega_k); \quad (94)$$

$$z_k=\frac{\left(\eta_k-f_\eta^{(k)}\right)\cos\eta_k l-\left(f_\eta^{(k)}/f_\xi^{(k)}\right)\left(\xi_k-f_\xi^{(k)}\right)\cos\xi_k l}{\left(\eta_k-f_\eta^{(k)}\right)\sin\eta_k l-\left(\xi_k-f_\xi^{(k)}\right)\sin\xi_k l} \quad (95)$$

Numerical results

The characteristics of the CF beam are as follows: $l = 7.62$ m, $A = 5.90 \times 10^{-3}$ m^2, $E = 2.14 \times 10^{11}$ N/m^2, $G = 8.18 \times 10^{10}$ N/m^2, $I = 4.58 \times 10^{-5}$ m^4, mass of beam, $m = 350$ kg, $\kappa = 5/6$. The calculation results are compared with the EB beam in [31], where their frequencies are determined by analytical solution:

$$\omega = \frac{\lambda^2}{l^2}\sqrt{\frac{EI}{\rho A}} \tag{96}$$

where λ is the solution of the characteristic Equation:

$$\cos\lambda \cosh\lambda + 1 = 0 \tag{97}$$

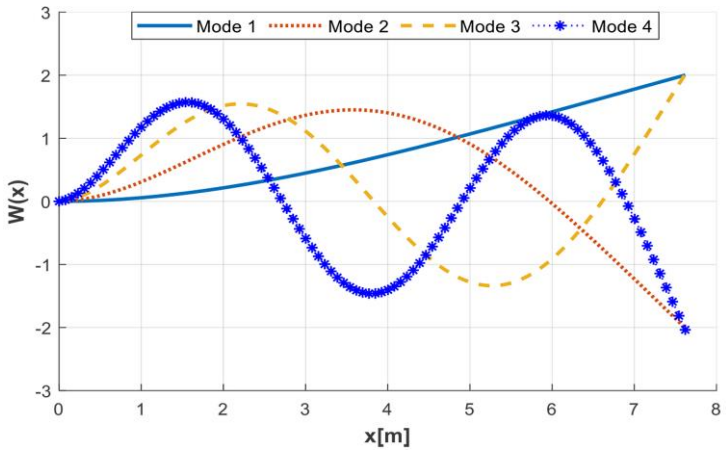

Figure 6. Mode shapes of the transverse displacement of the CF PTM beam

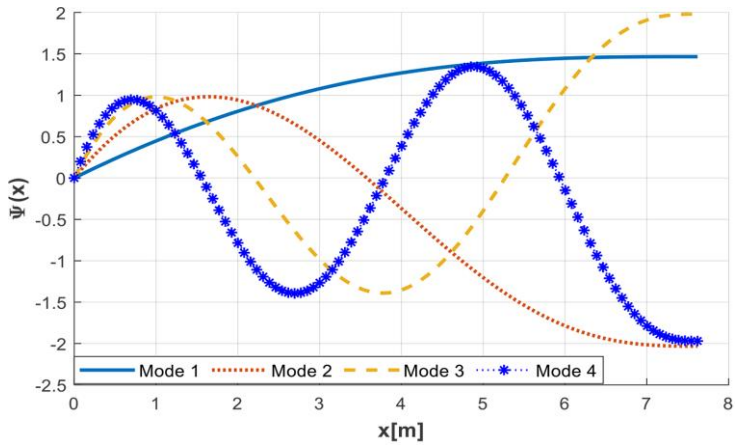

Figure 7. Mode shapes of the cross-sectional rotation of the CF PTM beam

The outcomes of the computation are indicated in Table 2. The mode shapes of transverse displacement and cross-sectional rotation of the CF PTM beam are illustrated in Figures 6 and 7, respectively. The findings shown in Table 2 demonstrate that as the frequency order changes, the change in the difference of natural frequencies in the CF PTM beam is similar to that of the SS PTM beam. The first natural frequency also exhibits the greatest discrepancy (about 6.23% corresponding to $\varepsilon_0 = -3\times10^{-4}$). The difference decreases rapidly as the order of the natural frequency increases. The mode shapes of the CF PTM beam under $\varepsilon_0 = -3\times10^{-4}$, as shown in Figures 6 and 7, are appropriate for this type of boundary condition.

Clamped-support PTM beam

Boundary conditions of clamped–support (CS) PTM beam are shown in Figure 8. At $x=0$, both displacement and rotation are zero.

Table 2. Natural frequencies of CF PTM beam (Hz)

No.	PTM (a), (Hz)			TM (b), (Hz)	EB [31], (Hz)	(a-b)/b (%)
	$\varepsilon_0 = -10^{-4}$	$\varepsilon_0 = -3.10^{-4}$	$\varepsilon_0 = 10^{-4}$	$\varepsilon_0 = 0$		
1	4.356362	4.166201	4.550521	4.443	4.451	6.23
2	27.34684	26.87677	28.1266	27.651	27.899	2.80
3	76.12447	75.92555	77.23382	76.507	78.119	0.76
4	147.1811	146.6947	148.0214	147.417	153.082	0.49
5	238.5178	237.8973	239.0906	238.661	253.057	0.32
6	347.8383	347.3198	348.5030	347.981	378.023	0.19
7	472.9603	472.3832	473.6794	473.0928	527.9831	0.15
8	611.6868	611.1239	612.3842	611.7969	702.9361	0.11
9	761.9678	761.3886	762.6613	762.0745	902.8825	0.09
10	922.1156	921.5734	922.5140	922.1267	1127.822	0.06

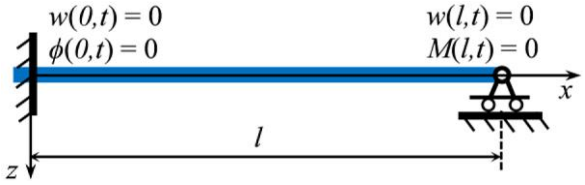

Figure 8. Clamped–support (CS) beam

$$w(0,t)=0 \Rightarrow W(0)=0;\ \phi(0,t)=0 \Rightarrow \Phi(0)=0 \tag{98}$$

At $x = l$, both displacement and moment are zero. Similar to the SS beam, we have:

$$W(l)=0, \Phi'(l)=0 \tag{99}$$

In frequency region $\omega < \omega_c$:
Natural frequency – by substituting Equation 52 and Equation 53 into Equation 98 and Equation 99. The characteristic equations to determine frequencies are:

$$\begin{aligned}&\left(\sinh\beta l-\left(h_\beta/f_\xi\right)\sin\xi l\right)\left(\beta h_\beta\cosh\beta l+\xi f_\xi\cos\xi l\right)\\&-(\cosh\beta l-\cos\xi l)\left(\beta h_\beta\sinh\beta l+\xi h_\beta\sin\xi l\right)=0\end{aligned} \tag{100}$$

$$W_j(x) = a_1^{(j)}\left(\sinh\beta_j x+g_j\cosh\beta_j x-\frac{h_\beta^{(j)}}{f_\xi^{(j)}}\sin\xi_j x-g_j\cos\xi_j x\right) \tag{101}$$

$$\Phi_j(x) = a_1^{(j)}\left(h_\beta^{(j)}g_j\sinh\beta_j x+h_\beta^{(j)}\cosh\beta_j x+f_\xi g_j\sin\xi_j x-h_\beta^{(j)}\cos\xi_j x\right) \tag{102}$$

where

$$h_\beta^{(j)}=h_\beta(\omega_j);\ f_\xi^{(j)}=f_\xi(\omega_j);\ \xi_j=\xi(\omega_j);\ \beta_j=\beta(\omega_j); \tag{103}$$

$$g_j=\frac{\left(h_\beta^{(j)}/f_\xi^{(j)}\right)\sin\xi_j l-\sinh\beta_j l}{\cosh\beta_j l-\cos\xi_j l} \tag{104}$$

In frequency region $\omega > \omega_c$:
Natural frequency – substituting Equation 56 and Equation 57 into the boundary conditions Equation 98 and Equation 99. The characteristic equation to determine the natural frequencies is:

$$\begin{aligned}&\left(\sin\eta l-\left(f_\eta/f_\xi\right)\sin\xi l\right)\left(-\eta f_\eta\cos\eta l+\xi f_\xi\cos\xi l\right)\\&-(\cos\eta l-\cos\xi l)\left(-\eta f_\eta\sin\eta l+\xi f_\eta\sin\xi l\right)=0\end{aligned} \tag{105}$$

Mode shape:

$$W_k(x) = b_1^{(k)}\left(\sin\eta_k x+z_k\cos\eta_k x-\left(f_\eta^{(k)}/f_\xi^{(k)}\right)\sin\xi_k x-z_k\cos\xi x\right) \tag{106}$$

$$\Phi_k(x) = b_1^{(k)} \left(-z_k f_\eta^{(k)} \sin \eta_k x + f_\eta^{(k)} \cos \eta_k x + z_k f_\xi \sin \xi_k x - f_\eta^{(k)} \cos \xi x \right) \quad (107)$$

where

$$f_\eta^{(k)} = f_\eta(\omega_k);\ f_\xi^{(k)} = f_\xi(\omega_k);\ \xi_k = \xi(\omega_k);\ \beta_k = \beta(\omega_k); \quad (108)$$

$$z_k = \frac{\left(f_\eta^{(k)} / f_\xi^{(k)} \right) \sin \xi_k l + \sin \eta_k l}{\cos \eta_k l - \cos \xi_k l} \quad (109)$$

Table 3. Natural frequencies of the CS PTM beam (Hz)

No.	PTM (Hz)				TM (Hz)	EB [31] (Hz)	(a-b)/b (%)
	$\varepsilon_0 = -1 \cdot 10^{-4}$	$\varepsilon_0 = -2 \cdot 10^{-4}$ (a)	$\varepsilon_0 = 1 \cdot 10^{-4}$	$\varepsilon_0 = 2 \cdot 10^{-4}$	$\varepsilon_0 = 0$ (b)		
1	19.042	18.680	19.744	20.086	19.396	19.522	3.69
2	61.770	61.366	62.569	62.964	62.171	63.264	1.29
3	127.273	126.857	128.100	128.511	127.687	131.995	0.65
4	213.626	213.209	214.458	214.873	214.043	225,720	0.39
5	318.628	318.213	319.455	319,867	319.041	344.438	0.26
6	439.987	439.578	440.803	441.211	440.395	488.150	0.19
7	575.474	575.073	576.277	576.677	575.875	656.854	0.14
8	880.780	880.394	881.550	881.935	881.165	850.552	0.09
9	1047.12	1046.74	1047.87	1048.255	1047.50	1069.24	0.07
10	1220.66	1220.29	1221.40	1221.768	1221.03	1312.92	0.06

Numerical results

The properties of the CS beam are similar to those of the CF beam. The calculation results are compared with the EB beam in [31], where the solution of the characteristic equation is:

$$\tan\lambda - \tanh\lambda = 0 \quad (110)$$

The results of natural frequency for different beams are indicated in Table 3. Mode shapes of displacement of the CS PTM beam and the relative error in natural frequencies between the CS PTM beam and CS TM beam are illustrated in Figures 9 and 10, respectively.

According to the findings in Table 3, the change in natural frequencies of the CS PTM beam presents the same tendency as the SS and CF PTM beams. The four mode shapes of the CS PTM beam under pre-compression ($\varepsilon_0 = -2 \cdot 10^{-4}$) are shown in Figure 9 and are consistent with this type of boundary condition. It can be seen in Figure 10 that the relative difference increases as the prestress increases and significantly decreases as the frequency order increases.

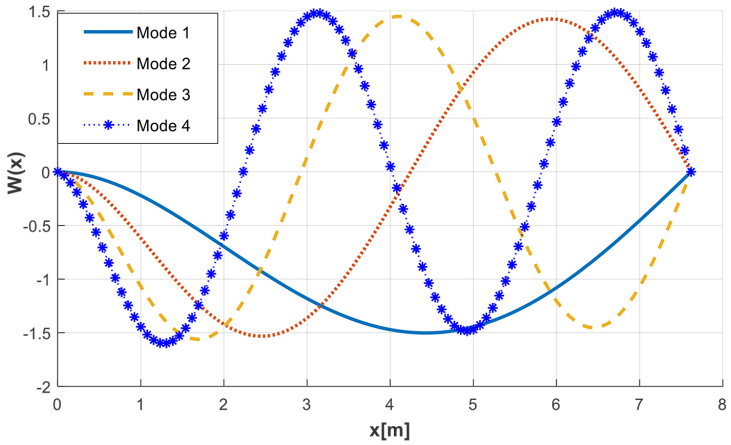

Figure 9. Mode shapes of displacement of CS PTM beam

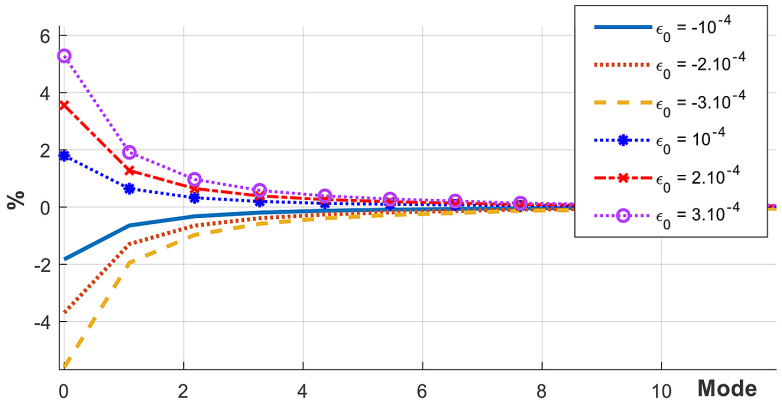

Figure 10. Relative error in natural frequencies between CS PTM beam and CS TM beam

CONCLUSIONS

This study employs the vibration equations developed for the Timoshenko beam and applies them to the prestressed Timoshenko beam using the modal analysis method. This study also investigates characteristic equations to identify the natural frequencies and mode shapes for distinct prestressed Timoshenko beam models, namely: simply supported beam, clamped-free beam, and clamped-support beam, using the general form of mode functions with specific boundary conditions. Other types of beams with different boundary conditions at the end edge can also be examined using the same method as described for the above boundary conditions.

Numerical calculations have been carried out for various beam models, and the results have been compared with Timoshenko beams and Euler-Bernoulli beams. The calculations yield similar results for Timoshenko beams when the prestress of the prestressed Timoshenko beams is zero. Additionally, the results show a good agreement with the Euler-Bernoulli beam.

When the beams are pre-compressed, as the prestress increases, the difference in natural frequencies of the prestressed Timoshenko beam increases compared to the Timoshenko beam. The natural frequency of the pre-tensioned beam is greater than that of the beam without pre-tensioning. The difference is most pronounced at the initial frequency and is considered the most significant. However, this difference diminishes rapidly as the frequency order increases.

In this study, the natural frequency of the prestressed PTM beam has been examined using the modal analysis method. However, it is possible to investigate the forced vibration of this beam using the same applied method. This investigation could be considered as a further study.

REFERENCES

1. Hagedorn P. and DasGupta A. Vibrations and waves in continuous mechanical systems. John Woley&Sons, 2007.
2. Leissa A.W. and Qatu M.S. Vibration of Continuous Systems. McGraw-Hill, 2011.
3. Bottega W.J. Engineering Vibrations. CRC Press, 2006.
4. Meirovitch L. Analytical Methods in Vibrations. The Macmillan Company, 1967.
5. Gere J.M. and Timoshenko S.P. Mechanics of Materials. PWS Engineering, 1984.
6. Karacam F. and Aydogdu M. Wave propagation characteristics in functionally graded double-beams. Advances in Science and Technology Research Journal, 2017; 11(3): 143–49. doi:10.12913/22998624/76697.
7. Majkut L. Free and forced vibrations of Timoshenko beams described by single difference equation. Journal of theoretical and applied mechanics, 2009; 47(1): 193–210,.
8. Kim T., Park I., and Lee U. Forced vibration of Timoshenko beam subjected to stationary and moving loads using the modal analysis method. Shock and Vibration, 2017; 1–26, doi: 10.1155/2017/3924921.
9. Azam S.E., Mofid M. and Khoraskani R.A. Dynamic response of Timoshenko beam under moving mass. Scientia Iranica, Transaction A: Civil Engineering, 2013; 20(1): 50–56. doi: 10.1016/j.scient.2012.11.003.
10. Amiri A.M., Olfati A., Najjar S., Beiranvand P., Fard M.H.N. Study on flexural of reinforced geopolymer concrete beam. Advances in Science and Technology Research Journal, 2016; 10(30): 89–95. doi:10.12913/22998624/62630.
11. Al-Baijat H., Alhawamdeh M., and Khawaldeh A. Studying the flexural behavior of reinforced concrete beams under the effect of high temperature: A finite element model. Advances in Science and

Technology Research Journal, 2019; 13(2): 150–56. doi:10.12913/22998624/109055.

12. Piotrowski R. and Siedlecka M. Point protection of primary beams of steel grillages against lateral torsional buckling. Advances in Science and Technology Research Journal, 2020; 14(3): 1–8. doi:10.12913/22998624/121532.
13. Zhang Y., Cheng Y., Tan G., Lyu X., Sun X., Bai Y., and Yang S. Natural frequency response evaluation for RC beams affected by steel corrosion using acceleration sensors. Sensors, 2020; 20(18): 1–17. doi:10.3390/s20185335.
14. Zhang L., Sun L., and Dong L. Experimental study on the relationship between the natural frequency and the corrosion in reinforced concrete beams. Advances in materials science and engineering, 2021; 1–10. doi: 10.1155/2021/9976738.
15. Barrias A., Rodriguez G., Casas J.R., and Villalba S. Application of distributed optical fiber sensors for the health monitoring of two real structures in Barcelona. Structure and Infrastructure Engineering, 2018; 14(7): 967–985. doi: 10.1080/15732479.2018.1438479.
16. Kaloop M.R. and Li H. Monitoring of bridge deformation using GPS technique. KSCE Journal of Civil Engineering, 2009; 13(6): 423–431. doi: 10.1007/s12205-009-0423-y.
17. Elhattab A., Uddin N., andObrien E. Drive-by bridge frequency identification under operational roadway speeds employing frequency independent underdamped pinning stochastic resonance (FIUPSR). Sensors, 2018; 18(12): 1–22. doi: 10.3390/s18124207.
18. Moradipour P., Chan T.H.T., and Gallage C. Benchmark studies for bridge health monitoring using an improved modal strain energy method. Procedia Engineering, 2017; 188: 194–200. doi: 10.1155/2017/3924921.
19. Magnon C., Galaup A., Rouffiac V., Opolon P., Connault E., Rosé M., Perricaudet M., Roche A., Germain S., Griscelli F., and Lassau N. Dynamic assessment of antiangiogenic therapy by monitoring both tumoral vascularization and tissue degeneration. Gene Therapy, 2007; 14(2): 108–117. doi: 10.1038/sj.gt.3302849.
20. Huong N.T.V., Nam N.S., Khang N.V. Numerical evaluation of the vibration response of a Timoshenko beam subjected to a moving force using the modal analysis approach, JST: Engineering and Technology for Sustainable Development, 2022; 32(1): 61–70, doi: 10.51316/jst.156.etsd.2022.32.1.9.
21. Roshandel D., Mofid M., and Ghannadiasl A. Modal analysis of the dynamic response of Timoshenko beam under moving mass. Scientia Iranica, Transaction A: Civil Engineering, 2015; 22(2): 331–344.
22. Abeles P.W. and Bardhan-Roy B.K. Prestressed Concrete Designer's Handbook. 3rd edition, CRC Press, 1981.
23. Keer A.D. On the dynamic response of a prestressed beam. Princeton University Research Report, 1973.
24. Keer A.D. On the dynamic response of a prestressed beam. Journal of Sound and Vibration, 1976; 49(4): 569–573.
25. Saiidi M., Douglas B., Feng S. Prestress force effect on vibration frequency of concrete bridges. Journal of Structural Engineering, 1994; 120(7): 2233–2341. doi: 10.1061/(ASCE)0733-9445(1994)120:7(2233).
26. Fengge L. and Zhao Y. Finite element analysis of natural vibration frequency for unbounded prestressed concrete beams. Applied Mechanics and Materials, 2013; 351–352: 1034–1037. doi: 10.4028/www.scientific.net/AMM.351-352.1034.
27. Huong N.T.V. and Dien N.P. On the natural frequency and mode shape of a cracked and prestressed beam. Journal of Science and Technology (Technical Universities), 2014; 103: 47–52.
28. Huong N.T.V., Khang N.V., and Dien N.P. Dynamic response of a cracked and prestressed beam under the action of a moving body. Journal of Science and Technology (Technical Universities), 2015; 106: 58–62.
29. Jiang J. and Ye G. Dynamics of a prestressed Timoshenko beam subject to arbitrary external load, Journal of Zhejiang University-SCIENCE A (Applied Physics & Engineering), 2010; 11(11): 898–907. doi: 10.1631/jzus.A1000057.
30. Kien N.D. Free vibration of prestress Timoshenko beams resting on elastic foundation. Vietnam Journal of Mechanics, 2007; 29(1): 1–12. doi: 10.15625/0866-7136/29/1/5586.
31. Inman D.J. Engineering Vibration, 4th edition, Upper Saddle River, 2014.
32. Khatir A., Capozucca R., Khatir S., and Magagnini E. Vibration-based crack prediction on a beam model using hybrid butterfly optimization algorithm with artificial neural network. Frontiers of Structural and Civil Engineering, 2022; 16(8): 976–989. doi:10.1007/s11709-024-1079-x.
33. Khatir A., Tehami M., Khatir S., and Wahab M.A. Multiple damage detection and localization in beam-like and complex structures using coordinate modal assurance criterion combined with firefly and genetic algorithms. Journal of Vibroengineering, 2016; 18(8): 5063–5073. doi: 10.21595/jve.2016.17026.
34. Raju P.M., Kumar M.P., Adiseshu S., and Kumar V.V.S.S. Mathematical Model for Natural Frequency of Prestressed Concrete beam using STAAD.Pro. In IOP Conference Series: Materials Science and Engineering, 1025(1): 012008, Vizianagaram, India, 15–16th November 2019. doi:10.1088/1757-899X/1025/1/012008.

35. Hamed E. and Frostig Y. Natural frequencies of bonded and unbonded prestressed beams-prestress force effects. Journal of Sound and Vibration, 2006; 29528–39. doi: 10.1016/j.jsv.2005.11.032.
36. Brecolotti M., Ubertini F., and Venanzi I. Natural frequencies of prestressed concrete beams: theoretical prediction and numerical validation. In: Proceeding of the XIX Aimeta Conference, 14–17, Ancona, Italy, 2009.
37. Belletti B. and Gasperi A. Behavior of prestressed steel beams. Journal of Structural Engineering, 2010; 136(9): 1131–39. doi:10.1061/(asce) st.1943-541x.0000208.
38. Gosaye J., Gardner L., Wadee M.A., and Ellen M.E. Compressive behaviour and design of prestressed steel elements. Structures, 2016; 5: 76–87. doi:10.1016/j.istruc.2015.09.001.
39. Hadjipantelis N., Gardner L., and Wadee M.A., A.M.ASCE. Finite-element modeling of prestressed cold-formed steel beams. Journal of Structural Engineering, 2019; 145(10): 1–19. doi:10.1061/(asce) st.1943-541x.0002375.
40. Hadjipantelis N., Gardner L., and Wadee M.A. Design of prestressed cold-formed steel beams. Thin-Walled Structures, 2019; 140: 565–78. doi:10.1016/j.tws.2019.02.029.
41. Reddy J.N. Energy principles and variational method in applied mechanics. John Wiley&Sons, 2002.